THE JOURNAL OF PHYSICAL CHEMISTRY C

Article

pubs.acs.org/JPCC

Confirmation of the Origins of Panchromatic Spectra in Squaraine Thin Films Targeted for Organic Photovoltaic Devices

Nicholas J. Hestand,[†] Chenyu Zheng,[‡,§,∥] Anirudh Raju Penmetcha,[‡] Brandon Cona,[‡] Jeremy A. Cody,[‡] Frank C. Spano,[†] and Christopher J. Collison*[,‡,§,∥]

[†]Department of Chemistry, 130 Beury Hall, 1901 N. 13th Street, Temple University, Philadelphia, Pennsylvania 19122, United States

[‡]School of Chemistry and Materials Science, [§]Nanopower Research Laboratory, and [∥]Microsystems Engineering, Rochester Institute of Technology, Rochester, New York 14623, United States

Supporting Information

ABSTRACT: Squaraines offer significant potential for organic photovoltaics because of their broad absorbance and high extinction coefficients as well as their expected use as mechanistic probes in such devices. In this work steps are taken to develop a comprehensive understanding of the excited-state properties of squaraines on the basis of their molecular structure and the resulting solid-state packing. Accurate assignments of the absorption spectral peaks are made on the basis of an essential states model, expanded to include intermolecular charge transfer (ICT). A comparison of simulated spectra with spectra for two symmetric squaraine derivatives confirms that ICT has a major influence on the optical and electronic properties of squaraine aggregates, fully accounting for the origin of the strong panchromaticity of these systems.

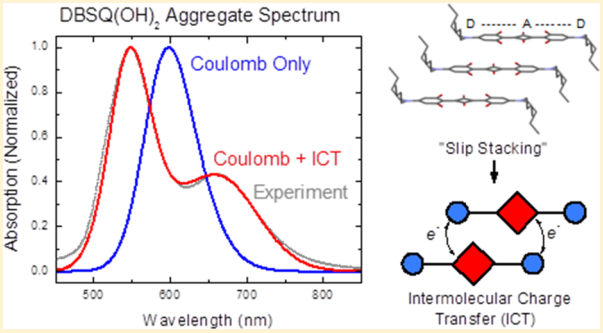

I. INTRODUCTION

Squaraines continue to be enthusiastically investigated for applications such as nonlinear optics,[1,2] two-photon fluorescence microscopy bioimaging,[3,4] and photodynamic therapy.[5,6] They typically exhibit sharp and intense near-infrared (NIR) absorption bands in solution (frequently associated with strong fluorescence) which become substantially broadened and often red-shifted in the solid state.[7] This strong panchromaticity coupled with high extinction coefficients (in excess of 10^5 L $mol^{-1}cm^{-1}$)[8] offers huge potential for squaraine-based organic photovoltaic (OPV) devices.[9−12]

The benefits of squaraines lie far beyond their panchromaticity in the solid state, however. The chemical space spanned by squaraine derivatives is vast, offering nearly endless possibilities for varying their structure to target more efficient prototypes which can be effectively mass produced. The golden synergy is to make materials capable of achieving high photovoltaic efficiencies while retaining the structural properties necessary for processing success: synthesis reproducibility, quality control, and solvation in nontoxic ink vehicles. Nevertheless, the key to optimizing their optoelectronic properties lies in a more fundamental appreciation of the origin of the panchromaticity. To this end, we must first develop a comprehensive understanding of the excited-state properties of squaraines based on their molecular structure and the resulting solid-state packing in pure and blended forms.

Understanding the nature of excited states in the solid phase (aggregates, thin films, and crystals) is critical for developing successful OPV devices. Schwenn et al.[13] and separately Coffey et al.[14] discuss the major driving forces for the generation of free carriers from excitonic states using Marcus−Hush theory. Furthermore, Spencer et al.[9] describe how Marcus−Hush theory can be used to explain why the increased crystallinity within squaraine devices has a detrimental effect on the donor−acceptor electron transfer rate, which appears to limit OPV device efficiency. In a system with a variety of aggregates and polymorphs, the intermolecular coupling between the multiple donors and the acceptor will vary depending on the electronic and spatial properties of those donor species.

Bigelow and Freund[15] performed semiempirical molecular orbital calculations on squaraine monomers, emphasizing the ground-state conformational and solution-phase spectroscopic properties. In solution, they describe a positively charged solvent cage surrounding the oxygen atoms and a negatively charged solvent cage surrounding the amino phenyls, inducing greater $D^{+/2}$-A$^-$-$D^{+/2}$ character within the ground state. The mixing of zwitterionic character within the ground state is also shown by Painelli and co-workers to be essential to describing symmetry breaking and solvochromism in a variety of quadrupolar dye molecules.[16] The calculations of Bigelow and Freund[15] suggest that the crystal structure of a hydroxysquaraine reveals an intermolecular packing consistent with these solvent interactions, i.e., the zwitterionic contribution in the crystal phase would be stabilized through intermolecular

Received: May 28, 2015
Revised: July 21, 2015
Published: July 22, 2015

DOI: 10.1021/acs.jpcc.5b05095
J. Phys. Chem. C 2015, 119, 18964−18974

electrostatic interactions in a manner similar to the stabilization achieved in solution via the formation of squaraine/solvent complexes.

Tristani-Kendra and Eckhardt[17] describe efforts to understand the origin of the panchromaticity, stating the challenges of comparing aggregates in solution with aggregates in crystals. They explain how total agreement is hard to find because of polymorphs that exist in the crystal; the polymorph pertaining to the aggregate in solution may not be spectroscopically dominant in the crystal. That work also describes how reflectivity data can be extremely different for two polymorphs reflecting widely differing packing structures and solid-state interactions. Notably, in the Kramers−Kronig absorption spectrum of the triclinic crystal of 1,3-bis[4-(*N*,*N*-diethylamino)-2-hydroxyphenyl]squaraine (DESQ(OH)), absorption polarized perpendicular to the molecular plane is attributed to an intermolecular charge transfer (ICT) transition. This assignment is justified by the slip-stacked packing arrangement which provides an ideal environment for ICT due to an interplanar spacing of 3.35 Å and spatially overlapping molecular orbitals at the donor (nitrogen) and acceptor (four-membered ring) moieties on neighboring molecules. Tanaka[18] describes how this slipped stack or "staircase" arrangement is favorable for charge resonance interactions for dye crystals in general. Conversely, no ICT transition is observed for the monoclinic polymorph of DESQ(OH) which exhibits a herringbone packing structure featuring spatially separate donor and acceptor moieties on neighboring molecules.

In more recent work, some confusion seems apparent regarding the origin of the panchromatic solid-state features when using typical assignments[10,11,19−22] based solely on the aggregation-induced spectral shifts,[23,24] where a red shift is characteristic of J aggregates and a blue shift is characteristic of H aggregates, as originally described by Kasha.[25] Thus, high-energy peaks might be attributed to the formation of H aggregates, and low-energy peaks may be attributed to J aggregates. Such an assignment is misleading considering that spectral shifts can arise from sources other than excitonic coupling.[24,26] The assignment also precludes the possibility of important ICT interactions, as Kasha theory is predicated on dominant Coulombic interactions alone.

In this article, we make a more accurate assignment of the peaks based on an essential states model pioneered by Painelli and co-workers.[16,27−32] The essential states model accounts for the charge transfer nature of the transitions within a given squaraine: each chromophore is described with two donor units (amine side arms) and a central squarylium acceptor unit. The essential states include three diabatic electronic states: the CT precursor state, DAD, and the two degenerate charge-separated states, D^+A^-D and DA^-D^+. An aggregate model based on Painelli's essential states offers many advantages over standard exciton theory, as it explicitly accounts for the molecular polarizability through mixing among the diabatic states.[28−32] Although the exciton number is no longer a good quantum number as it is in Frenkel exciton theory under the Heitler−London approximation,[33] the essential states aggregate model provides a more accurate account of ground- and excited-state supramolecular properties[28−32] and permits a description of exotic phenomena such as symmetry breaking and solvatochromism.[16,27] As we will show, the model also allows for an intuitive description of intermolecular charge transfer reactions between closely π-stacked squaraine aggregates, consistent with the interpretations made by Tristani-Kendra and Eckhardt.[17]

Our work confirms that the ICT has a major influence on the optical and electronic properties of squaraine aggregates, fully accounting for the origin of the strong panchromaticity of these systems. This will allow the opportunity to explain orientational broadening in thin-film spectroscopic data.[34] With a full understanding of the nature of the excited states in squaraine aggregates, we provide a foundation to recognize the critical impact of controlling aggregation toward higher efficiencies of OPV devices, which rely on a fast rate of charge transfer at the bulk heterojunction interface.

II. EXPERIMENTAL SECTION

II.1. Synthesis. Following a modified procedure by Dirk et al.,[35] the preparation of symmetric squaraine dyes is generally straightforward when the starting amine can be readily purchased, albeit low-yielding. The general synthesis involves a one-pot, two-step protocol whereby a secondary amine is condensed at reflux with 1,3,5,-trihydroxybenzene in a 3:1 toluene/*n*-butanol solution. After cooling, a half equivalent of squaric acid is added and the mixture is heated to reflux. During both steps the water formed is azeotropically removed using a Dean−Stark trap. We prepared $DBSQ(OH)_2$[35] and $DPrSQ(OH)_2$[36] (Figure 1) following the general procedure above.

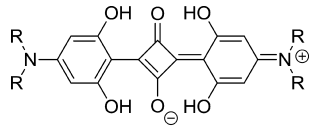

$DPrSQ(OH)_2$: R = *n*-propyl
$DBSQ(OH)_2$: R = *n*-butyl

Figure 1. Molecular structure of $DPrSQ(OH)_2$ and $DBSQ(OH)_2$.

Upon solvent exchange into cyclohexane, quality crystals suitable for X-ray analysis were readily obtained. Each squaraine product was consistent with the ^{1}H NMR spectral data previously reported.[35,36]

II.2. Spectral Characterization. The absorption measurements were carried out using a Shimadzu UV-2100PC spectrophotometer. The steady-state fluorescence was measured using a HORIBA FluoroMax fluorometer. Dimethyl sulfoxide (DMSO) was purchased from Fisher Chemical. Chloroform was purchased from Sigma-Aldrich. Both solvents were used as received. Squaraine stock solutions were bath sonicated before diluting to the desired concentrations. Squaraine films were made by spin coating the chloroform solution with a squaraine concentration of 8 mg/mL onto a PEDOT/PSS-coated, precleaned ITO substrate to resemble the real OPV device architecture. ITO-coated glass substrates were cleaned in ultrasonic baths of acetone and isopropyl alcohol for 30 min. A PEDOT/PSS dispersion was spin-cast onto the precleaned substrates at a spinning speed of 5000 rpm. Chloroform solutions were made and bath sonicated and then were spin coated at a speed of 800 rpm. The PEDOT/PSS-coated ITO substrate was used to properly set the baseline of the instrument. In the mixed solvent study, the stock solutions were made by dissolving squaraines into DMSO at a concentration of 1 mg/mL, and a series of blank solvent blends were prepared with varying DMSO/H_2O ratios. The final solution was made by injecting the stock solution into the blank solvent blends during sonication (300 μL of stock was dispersed into each of the 10 mL solvent blends). The pure blank solvent blends were used to set the baseline of the

DOI: 10.1021/acs.jpcc.5b05095
J. Phys. Chem. C 2015, 119, 18964−18974

Table 1. Unit Cell Dimensions Measured for a 0.50 × 0.14 × 0.06 mm^3 $DPrSQ(OH)_2$ Single Crystal and a 0.50 × 0.10 × 0.04 mm^3 $DBSQ(OH)_2$ Single Crystal

compound	a/Å	b/Å	c/Å	α/deg	β/deg	γ/deg
$DPrSQ(OH)_2$	5.215(2)	10.894(4)	11.156(5)	101.345(8)	95.099(9)	100.549(8)
$DBSQ(OH)_2$	5.169(4)	10.846(9)	13.538(11)	77.165(19)	79.143(14)	76.324(14).

instrument before taking the absorption measurement for each corresponding mixed-solvent solution.

II.3. Crystallography. The single-crystal structures were determined on a Bruker SMART APEX II CCD Platform diffractometer at 100.0(5) K. The crystal was placed onto the tip of a 0.1-mm-diameter glass capillary tube or fiber. The structure was solved using SIR2011 and refined using SHELXL-2014. Space group *P*1 was determined on the basis of intensity statistics. The full data collection was carried out using Mo Kα radiation (λ = 0.71073 Å) with a frame time of ~60 s and a detector distance of 4.0 cm. The sizes of the $DPrSQ(OH)_2$ and $DBSQ(OH)_2$ crystals were 0.50 × 0.14 × 0.06 and 0.50 × 0.10 × 0.04 mm^3, respectively. Unit cell dimensions are provided in Table 1.

III. RESULTS AND DISCUSSION

The absorption spectra of $DPrSQ(OH)_2$ and $DBSQ(OH)_2$ in dilute chloroform solution and in a neat thin film are shown in Figure 2. The solution spectra are typical of all squaraines with

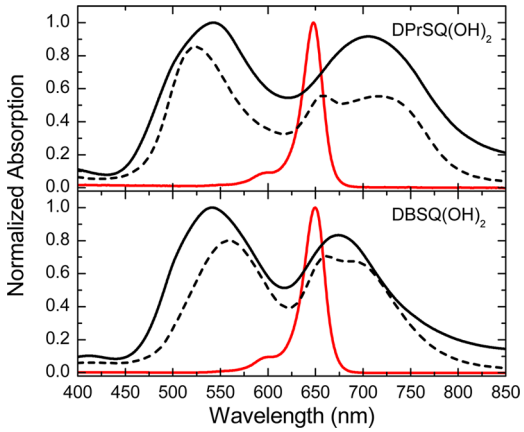

Figure 2. Normalized UV−vis absorption spectra of $DPrSQ(OH)_2$ (top panel) and $DBSQ(OH)_2$ (bottom panel) in dilute chloroform solution (red line), as a thin film (black solid line) and in a DMSO/H_2O mixed solvent solution (black dashed line). Note that the films were annealed at 150 °C for 1 min to drive aggregates toward their thermodynamic minimum, analogous to the aggregates in mixed-solvent solutions and single crystals.

narrow monomer peaks at 648 and 650 nm and full width at half maxima (fwhm) of 0.073 and 0.081 eV for $DPrSQ(OH)_2$ and $DBSQ(OH)_2$, respectively. For each squaraine there is a weak vibronic shoulder at 600 nm. The extinction coefficient for each squaraine in chloroform solution was characterized to be (4.2 ± 0.1) × 10^5 cm^{-1} M^{-1} for $DPrSQ(OH)_2$ and (3.0 ± 0.1) × 10^5 cm^{-1} M^{-1} for $DBSQ(OH)_2$. For the $DPrSQ(OH)_2$ film, the high-energy peak at 547 nm is blue-shifted from the monomer peak in solution by 101 nm (0.354 eV) with an estimated fwhm of 0.53 eV. The low-energy peak in the film is at 705 nm, red-shifted by 57 nm (0.156 eV) from the monomer peak, with a fwhm estimated to be 0.28 eV. For $DBSQ(OH)_2$, the high-energy peak is at 543 nm, blue-shifted by 107 nm (0.376 eV) from the monomer peak in solution. The low-energy peak is at 673 nm, red-shifted by 23 nm (0.065 eV) from the monomer peak in solution. The fwhm's of high-energy and low-energy peaks in $DBSQ(OH)_2$ thin-film absorption spectra are estimated to be 0.626 and 0.413 eV, respectively. We summarize that both squaraine films have two absorption features blue- or red-shifted from the monomer, both with broader profiles.

The broadening of the absorption spectrum into a double-hump absorption is often found in similar anilinic squaraines with linear *N*-alkyl molecular arms.[9−11,19−22] The high-energy peak has been assigned to H-aggregate formation consistent with the literature.[9−11,19,20,22] The assignment of the low-energy peak is somewhat controversial. Chen[12] and Brück[37] both assigned the low-energy peaks to J-aggregate formation in the solid state based solely on the spectral shifts. However, a conflicting observation, inconsistent with this assignment, is that this J-aggregate is nonfluorescent. Of course, the H-aggregate is not expected to fluoresce because of Kasha's rule relaxation, leading to the population of the dark exciton at the bottom of the band. In all of our measurements, no fluorescence is detected for either $DPrSQ(OH)_2$ or $DBSQ(OH)_2$ films, regardless of which absorption feature is excited.

Liang et al.[38] state that, in their samples, the formation of the red-shifted aggregate is attributable to an "orientation effect", initiated through increasing temperature. The aggregate responsible for the blue-shifted peak is regenerated when the red-shifted aggregates are subjected to a steam treatment. Importantly, the assignment of red-shifted features to the J-aggregate seems to be made tentatively, based on qualitative assignments made elsewhere.[39−41]

As illustrated above and, indeed, from simple interpretations of our thin-film annealing data, the assignment of the low-energy feature is speculative. The impact of thermal annealing thin films of $DBSQ(OH)_2$ is shown in Figure 3a. Of note, the higher-energy peak blue shifts from 565 to 541.5 nm (0.095 eV), and the lower-energy peak further red shifts from 652 to 674 nm (0.062 eV). One might reasonably interpret the change as resulting from a closer interfacial spacing in the bulk of the material, leading to a larger Davydov splitting, consistent with an exciton model interpretation,[25] but we look to test this through our calculations below.

In contrast, when the films of $DPrSQ(OH)_2$ are annealed, there is far less of a shift (Figure 3b). The major difference is the relative increase in intensity of the blue-shifted peak as the annealing temperature is increased. We consider the possible causes for the relative change in intensity between these peaks. This change is different from the relative increase in the red-shifted peak observed for 1,3-bis[4-(*N*,*N*-diisopentylamino)-2,6-dihydroxyphenyl]squaraine ($DiPSQ(OH)_2$)[11] but is similar in that the change in the spectrum is likely linked to increased packing stability from higher populations of a more stable conformation after annealing. Nevertheless, the origins of a relative change in peak height are not clear. Moreover, each film is likely made up of a large distribution of aggregate sizes with a range of different intermolecular orientations; therefore, this

DOI: 10.1021/acs.jpcc.5b05095
J. Phys. Chem. C 2015, 119, 18964−18974

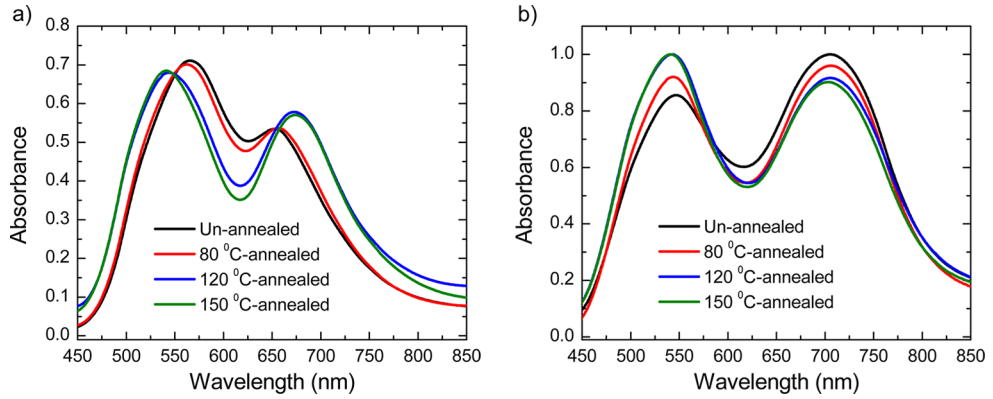

Figure 3. Absorption spectra of (a) $DBSQ(OH)_2$ and (b) $DPrSQ(OH)_2$ films as a function of annealing temperature; the annealing time for each temperature is 1 min.

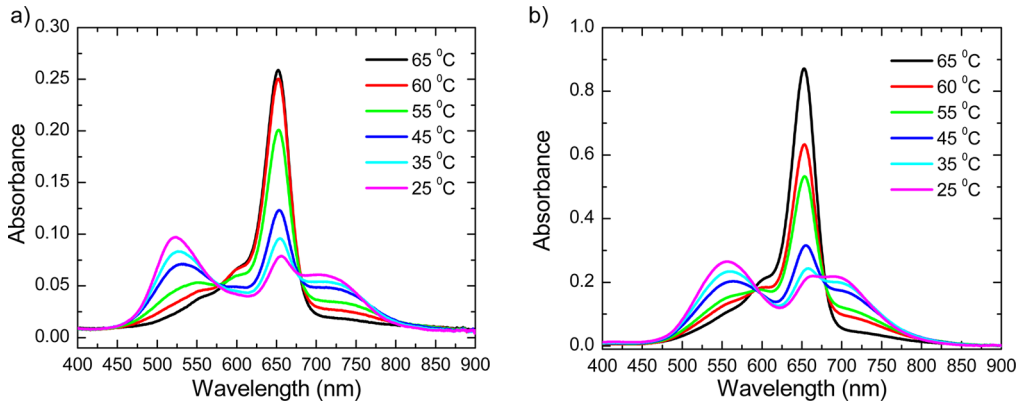

Figure 4. Absorption spectra of 72% DMSO/28% H_2O (by volume) for (a) $DPrSQ(OH)_2$ and 80% DMSO/20% H_2O (by volume) for (b) $DBSQ(OH)_2$ as a function of temperature.

uncertainty poses problems for a tight and conclusive interpretation.

In order to assign the absorption features with more confidence, it is necessary to visualize the transition of squaraine from monomer to aggregate. Only monomer absorption is observed for the squaraine solution as shown in Figure 2. However, the aggregation of squaraine is considered nearly complete in the as-cast films, and as just described, the aggregate distribution is large. Therefore, we turn our attention to aggregates formed in mixed solvents where the distribution of particle sizes is expected to be narrower and is based on the equilibrium that exists between monomer and aggregate, dependent on the specific solvent quality or temperature.

A comparison is made between the $DPrSQ(OH)_2$ thin-film absorption spectrum (Figure 2 top panel, black solid line) and the absorption spectrum of a thermodynamically stable aggregate[42] from a mixed-solvent nanoparticle dispersion (Figure 2 top panel, black dashed line). The peaks of the mixed-solvent system are observed at 525 and 718 nm, corresponding well to thin-film peaks at 542 and 705 nm. A similar comparison is made for $DBSQ(OH)_2$ where the thin-film spectrum (Figure 2 bottom panel, black solid line) is shown to overlap well with the mixed-solvent spectrum (Figure 2 bottom panel, black dashed line). We therefore claim that the aggregates in the mixed-solvent solutions of $DPrSQ(OH)_2$ and $DBSQ(OH)_2$ are analogous to the broad set of aggregates responsible for thin-film spectral features.

In the mixed-solvent work, we dissolve the squaraine in a mixture of solvents containing DMSO and H_2O. DMSO is a good organic solvent with a high solubility for squaraine monomer and is miscible with H_2O to form a uniform solvent environment.[43] The transition from monomer to aggregate as solvent quality is changed is demonstrated spectroscopically in Figure S1 for each squaraine, $DPrSQ(OH)_2$, and $DBSQ(OH)_2$. The photoluminescence spectra of these mixed-solvent solutions can be found in Figure S2. Only monomer fluorescence is observed until the DMSO content reaches a point where the monomer absorption almost disappears for each case, at 76% DMSO for $DBSQ(OH)_2$ and 68% DMSO for $DPrSQ(OH)_2$. Below these DMSO volume percentages, no fluorescence is observed regardless of the excitation wavelength. We restate how the lack of fluorescence contradicts an assignment of the low-energy peak to a J-aggregate, and we present an alternative, more accurate assignment, below.

Using solvent mixtures of 70% DMSO/30% H_2O (by volume) for $DPrSQ(OH)_2$ and 80% DMSO/20% H_2O (by volume) for $DBSQ(OH)_2$, the absorption spectra show the coexistence of monomers and aggregates (Figure 4). The mixed-solvent solutions were heated to 65 °C, and with increasing temperature, the squaraines are entropically driven to separate from aggregates into monomers. As the temperature increases from 25 to 65 °C, a gradual increase in monomer absorption is observed with a concomitant decrease in absorption at ~540 and ~710 nm, leaving two isosbestic points at 578 and 680 nm for $DPrSQ(OH)_2$ and two isosbestic points at 595 and 672 nm for $DBSQ(OH)_2$. For each squaraine, these isosbestic points confirm the interrelation between

DOI: 10.1021/acs.jpcc.5b05095
J. Phys. Chem. C 2015, 119, 18964−18974

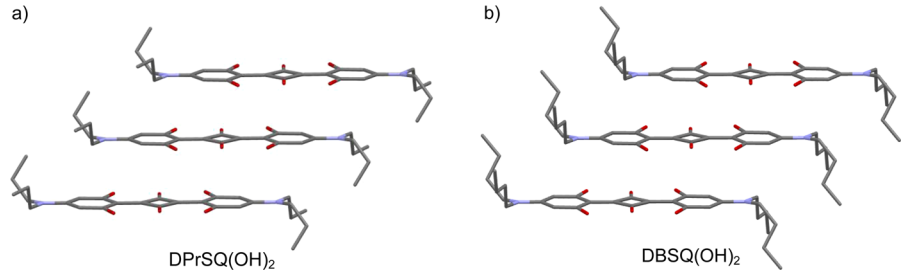

Figure 5. Single-crystal packing structures of (a) $DPrSQ(OH)_2$ and (b) $DBSQ(OH)_2$.

monomer and aggregate, with each aggregate spectrum showing the double-hump feature.

The data supports our conclusion that aggregates observed in mixed solvents are analogues of aggregates in thin film. In order to draw conclusions regarding a thermodynamically stable aggregate formed in solution and in the film, we have measured the analogous single-crystal structure through X-ray diffraction.

Both crystal structures are triclinic and display a very similar stacking motif, as shown in Figure 5, with full structural information provided in the SI. The planar distances of the $DPrSQ(OH)_2$ and $DBSQ(OH)_2$ crystals are both approximately 3.3 Å, and intramolecular hydrogen bonding is observed.

The molecular backbone (i.e., phenyl-squarylium-phenyl) is planarized by intramolecular hydrogen bonds between the phenyl ring hydroxyl groups and the squaric core oxygens. Both crystal structures highlight the slipped stack that comfortably fits the long *N*-alkyl molecular arms and, at the same time, enables short interplanar spacing. This face-to-face stacking suggests Coulombic interactions that are consistent with H-aggregate formation, an assignment supported by the blue-shifted peaks in the absorption spectra of thin films (Figure 2) and mutually agreed upon throughout the literature as described above.

We also note that the nitrogen atoms on neighboring molecules are very close to the squarylium ring. This packing motif highlights the possibility of intermolecular charge transfer between the positively charged nitrogen on a neighboring molecule to a negatively charged squarylium carbonyl. Hence, we now put forward a hypothesis that the ubiquitous double hump in the absorption spectra of these dihydroxy squaraines is largely due to the mixing between Frenkel-like exciton states and charge-separated states via ICT. We fully test this hypothesis with an applied theoretical construct, described below.

IV. THEORY

IV.1. Monomers. An essential states model describing donor−acceptor−donor (DAD) quadrupolar dyes has been developed by Painelli and co-workers in recent years.[16,27−32] Within the essential states framework, illustrated in Figure 6, each chromophore is modeled as a trio of diabatic electronic states, one representing each charge resonance structure of the dye: D^+A^-D ($|Z_1\rangle$), DAD ($|N\rangle$), and DA^-D^+ ($|Z_2\rangle$). For symmetric squaraines, the two zwitterion states, $|Z_1\rangle$ and $|Z_2\rangle$, are degenerate and separated from the neutral state, $|N\rangle$, by an energy $\eta_z > 0$. (Note that our notation differs slightly from that of Painelli.) The zwitterion states couple to the neutral state through the electron transfer integral t_Z, representing the movement of an electron between a nitrogen atom on one arm and the central four-membered ring. Hence, the electronic

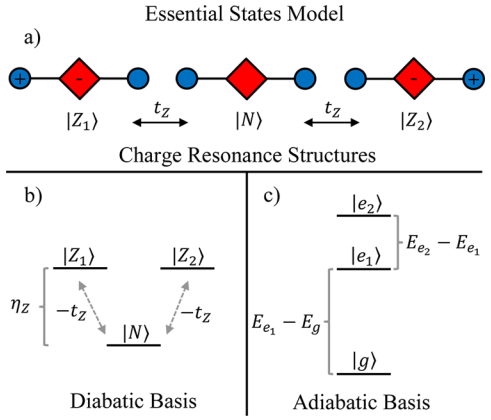

Figure 6. Illustration of the electronic basis states of the essential states model for a quadrupolar chromophore. (a) Resonance structures considered in the essential states model for squaraine chromophores. In the cartoon, the red squares represent the central four-membered ring of a squaraine molecule while the blue circles represent the nitrogen atoms on each arm. (b) Energy-level diagram of the diabatic basis states along with the matrix elements connecting them. (c) The eigenstates of a single chromophore determine the molecular properties, including optical absorption which involves the light-induced transition from the ground state $|g\rangle$ to the first excited state $|e_1\rangle$. The second excited state, $|e_2\rangle$, is two-photon-allowed.

Hamiltonian for the monomeric system is given in the local diabatic basis as

$$H_{\mathrm{el}}^{\mathrm{mon}} = \eta_Z \sum_{a=1,2} |Z_a\rangle\langle Z_a| - t_Z \sum_{a=1,2} (|N\rangle\langle Z_a| + hc) \quad (1)$$

which can be straightforwardly diagonalized to give the electronic eigenstates of the chromophore[27]

$$|g\rangle = \sqrt{1-\rho}\,|N\rangle + \sqrt{\rho/2}\,(|Z_1\rangle + |Z_2\rangle) \quad (2a)$$

$$|e_1\rangle = \sqrt{1/2}\,(|Z_1\rangle - |Z_2\rangle) \quad (2b)$$

$$|e_2\rangle = \sqrt{\rho}\,|N\rangle - \sqrt{(1-\rho)/2}\,(|Z_1\rangle + |Z_2\rangle) \quad (2c)$$

where parameter ρ defines the quadrupolar character of the ground state and is given by $\rho = 0.5(1 - \eta_Z/(\eta_Z^2 + 8t_Z^2)^{1/2})$. The corresponding energies, found by taking the expectation value of the Hamiltonian in eq 1, are given by $E_g = \rho\eta_Z - 2t_Z(2\rho(1-\rho))^{1/2}$, $E_{e_1} = \eta_Z$, and $E_{e_2} = (1-\rho)\eta_Z + 2t_Z(2\rho(1-\rho))^{1/2}$.

The model also accounts for vibronic coupling by introducing a vibrational mode with energy $\hbar\omega_{\mathrm{vib}}$ for each arm. The nuclear geometry of each arm is represented as a harmonic potential with the equilibrium point (arm length) defined by the electronic state of the system; when the system

DOI: 10.1021/acs.jpcc.5b05095
J. Phys. Chem. C 2015, 119, 18964−18974

is in a zwitterion state, the potential well of the arm hosting the zwitterion is shifted to a new equilibrium point relative to that of the neutral state. The difference in geometry between the neutral and zwitterion states is quantified by the Huang−Rhys parameter, λ^2, which defines the magnitude of the vibronic coupling. Hence, the vibronic Hamiltonian for a monomer is written as

$$\hat{H}^{\mathrm{mon}} = \hat{H}_{\mathrm{el}}^{\mathrm{mon}} + \hat{H}_{\mathrm{vib}}^{\mathrm{mon}} + \hat{H}_{\mathrm{el-vib}}^{\mathrm{mon}} \quad (3)$$

where $\hat{H}_{\mathrm{vib}}^{\mathrm{mon}}$ describes the intramolecular vibrational energy and $\hat{H}_{\mathrm{el-vib}}^{\mathrm{mon}}$ describes the vibronic coupling. Explicit forms of the vibrational and vibronic terms are given in the SI. Using the Hamiltonian in eq 3, Painelli and co-workers have successfully described the low-energy photophysics of both symmetric and antisymmetric squaraine dyes in solution.[16,27]

In order to parametrize the essential states Hamiltonian of eq 3 for $DPrSQ(OH)_2$ and $DBSQ(OH)_2$ monomers in solution, we compared our calculated absorption spectrum for each molecule with the experimentally measured spectrum. (Details of our calculation can be found in the SI.) In accordance with Painelli's results[27] for a similar squaraine, 1,3-bis[4-(*N*,*N*-dimethylamino)-phenyl]squaraine (DMSQ), we set t_Z = 1.05 eV while taking a slightly higher value of λ^2 = 1, typical of the vinyl stretching mode in conjugated organic molecules. We further set $\hbar\omega_{\mathrm{vib}}$ = 0.16 eV, consistent with the experimentally measured vibronic spacing, and adjusted the energy of the diabatic zwitterion states until our simulations reproduced the experimental spectrum. This procedure gave η_Z = 0.69 eV for the best-fit spectrum. For all monomer calculations, we have applied a Gaussian line shape function with a standard deviation of 0.06 eV. Figure 7 compares the simulated monomer spectra with experiment, showing that a good fit is obtained using these parameters. The experimentally measured monomer spectra of $DPrSQ(OH)_2$ and $DBSQ(OH)_2$ are nearly identical, which is not surprising considering that the main chromophore unit remains unchanged so that the same intramolecular parameters are taken for both species. The monomer spectrum is characterized by a vibronic progression with a dominant 0−0 peak, followed by much weaker side bands. It is quite interesting that an HR factor of unity for the vibronic coupling within each "arm" does not lead to a vibronic progression with roughly equal 0−0 and 0−1 intensities, as would be expected of the Poissonian progression with λ^2 = 1. The monomer spectrum is characterized by a much smaller effective HR factor due to charge delocalization over both arms, an effect which mimics J-aggregation.[44]

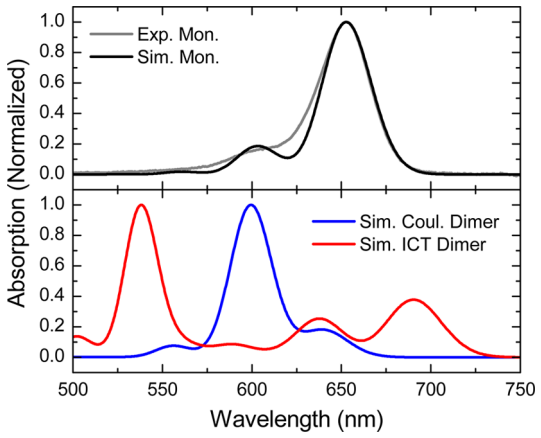

Figure 7. Simulated monomer (top panel) and dimer aggregate (bottom panel) spectra of $DPrSQ(OH)_2$. The top panel compares the experimental and simulated monomer spectra in solution; a good simulation fit validates the model parameters. In the bottom panel, the blue curve is evaluated using eq 4 where only Coulomb interactions between molecules are considered; the vibronic behavior expected of H-aggregates as predicted from exciton theory is observed as the vibronic intensity shifts to the higher vibronic peaks. The red curve, simulated using eq 5, illustrates the effect of ICT. Notably, several new red-shifted features appear, reminiscent of the experimental spectrum. The simulated $DBSQ(OH)_2$ spectra (not shown) look nearly identical. Note that each spectrum has been normalized to the most intense peak. Parameters for all calculations are given in the text.

IV.2. Coulombically Coupled Aggregates. Painelli and co-workers also studied the implications of Coulomb interactions between quadrupolar molecules undergoing aggregation.[28−32] This is achieved by accounting for the Coulomb interaction between molecules in zwitterionic states; the zwitterion charge densities are collapsed to positive and negative point charges residing on the nitrogen atoms and at the center of the four-membered ring, respectively, from which the Coulomb interaction can be calculated given the aggregate geometry. Our simulations confirm that this approach produces the characteristic vibronic spectral features exhibited by J- and H- aggregates as predicted by exciton theory.[23] The aggregate Hamiltonian accounting for the Coulomb interaction can be written as the sum of the monomer Hamiltonians and the Coulomb term $\hat{V}$ (see eq S.10 in the SI for the explicit form of $\hat{V}$), which is diagonal in the diabatic basis,[28,30]

$$\hat{H}_{\mathrm{Coul}}^{\mathrm{Agg}} = \sum_n \hat{H}_n^{\mathrm{mon}} + \hat{V} \quad (4)$$

Here $\hat{H}_n^{\mathrm{mon}}$ is the monomer Hamiltonian for the nth chromophore. While the Coulomb interaction impacts only the diagonal elements of the Hamiltonian when expressed in the diabatic basis, rotation into the adiabatic basis that diagonalizes $\sum_n \hat{H}_n^{\mathrm{mon}}$ transforms these interactions to the more familiar terms responsible for energy transfer between molecular sites. In the adiabatic basis, the Coulomb term appears in both diagonal and off-diagonal elements of the Hamiltonian. The off-diagonal terms coupling degenerate states are the same terms that serve to couple molecular excitons in exciton theory. For example, when the intermolecular separation R is large, the familiar point-dipole coupling expression which scales as R^{-3} is recovered. Additionally, there are off-resonance Coulomb terms which account for the molecular polarizability by allowing states having different numbers of excitations to mix. Furthermore, in the adiabatic basis, there remain diagonal Coulomb contributions to the Hamiltonian which can lead to stabilized multiexciton states, introducing the possibility of exciton strings.[30,45]

While the essential states model has been used to successfully simulate a variety of squaraine spectra, we find that, in its original form and using measured crystallographic geometries to determine electrostatic interactions, it cannot reproduce the mixed solvent or thin-film spectra of the two squaraines presented in Figure 2. Figure 7 shows the simulated absorption spectra of a $DPrSQ(OH)_2$ dimer aggregate when the molecules are allowed to interact Coulombically through $\hat{V}$ in eq S.10. The aggregate spectra are calculated by considering a squaraine dimer positioned at a geometry consistent with the crystal structures, which we assume to be the most stable conformation in the solvent mixtures as justified above. The position of the molecules relative to one another determines

DOI: 10.1021/acs.jpcc.5b05095
J. Phys. Chem. C 2015, 119, 18964−18974

their Coulomb interaction, which we have scaled by a dielectric of $\varepsilon = 3$ to account for the screening effects not explicitly included in the model. We note that the dimer system cannot be expected to account for the entirety of the aggregate photophysics due to its finite size; however, it is the simplest system that allows for intermolecular interactions. Simulations of larger aggregates, consisting of rigid chromophores due to computational restraints, do not significantly alter the conclusions drawn from the dimer system. Thus, the dimer is used as a simple model to gain insight into the effects of aggregation on the spectra. With this in mind, while we strive to maintain realistic parameters for intermolecular interactions, the parameters should be understood to be effective.

The simulated Coulombically coupled dimer spectrum, shown in Figure 7, exhibits the hallmark features of H-aggregation: the spectrum is blue-shifted and the vibronic intensity is redistributed from the 0−0 peak to the 0−1 peak. Nevertheless, these simulations fail to account for the substantial low-energy features observed in the measured squaraine spectra of Figures 2−4.

While several explanations can be given to account for the origin of the spectral line shape in $DPrSQ(OH)_2$ and $DBSQ(OH)_2$ aggregates consistent with Coulomb terms dominating the intermolecular interactions, we find that these arguments contradict experimental data. For instance, one might reasonably interpret the two dominant peaks in Figure 2 as upper and lower Davydov components. However, this interpretation contradicts the crystal structures of both $DPrSQ(OH)_2$ and $DBSQ(OH)_2$ which show only a single chromophore per unit cell. Davydov splitting requires at least two molecules per unit cell with inequivalent molecules having nonparallel transition dipole moments so that absorption to both the symmetric and antisymmetric exciton states is allowed. Furthermore, the presence of isosbestic points in the temperature studies (Figure 4) suggests that a single aggregated species is responsible for the double-hump behavior, thereby ruling out multiple aggregate hypotheses. We thus conclude that a new mechanism acting within a single aggregate species and consistent with the crystal structure is required to explain the photophysical behavior of $DPrSQ(OH)_2$ and $DBSQ(OH)_2$ aggregates.

IV.3. Intermolecular Charge Transfer Aggregates. As mentioned above, ICT has been suggested to be favorable in related squaraine materials due to the slip-stacked crystal packing that places the nitrogen atom of one molecule in closer proximity to the center of the four membered ring of its neighbor.[17,18,46] The crystal structures of both $DPrSQ(OH)_2$ and $DBSQ(OH)_2$ show the same overlapping behavior (Figure 5), suggesting that these systems are candidates for a similar ICT interaction. Such an ICT state is expected to affect the optical properties of the material as it couples directly to the optically active exciton state within the monomer. We assert that ICT is responsible for the double-hump behavior observed in the measured absorption spectrum.

To test this hypothesis, we extended the essential states model to allow for electron transfer between donor and acceptor moieties on neighboring molecules. (We note here that a similar approach describing intermolecular charge transfer was taken by Guasch et al.,[47] although this was used to describe the optical and ESR spectra of tetrathiafulvalene−triphenylmethyl dimers.) ICT necessitates including four additional diabatic states to represent the possible configurations of the ionized monomer: D^+AD ($|C_1\rangle$), DAD^+ ($|C_2\rangle$), DA^-D ($|A\rangle$), and $D^+A^-D^+$ ($|Z_3\rangle$). The ionic states arise due to the transfer of an electron between neighboring molecules via the spatially overlapping donor and acceptor moieties. Since we consider neutral excitations, anions and cations must always exist in pairs; the resulting charge transfer states are product states of an anion and a cation. We define the energy of an infinitely separated cation and anion pair consisting of $|C_1\rangle$ (or $|C_2\rangle$) and $|A\rangle$ chromophores to be η_{CT}. For simplicity, we approximate the energy of an infinitely separated $|Z_3\rangle$ and $|A\rangle$ pair to be $\eta_{CT} + \eta_Z$, adding the energy required to create a zwitterion on the neutral arm of a cation in a $|C_1\rangle$ (or $|C_2\rangle$) and $|A\rangle$ charge-separated pair. While this approximation is not rigorous, it reduces the number of adjustable parameters and should be a suitable estimate for the energy of the pair. The total energy of a charge- separated state also includes the distance-dependent Coulomb interaction through Coulomb operator $\hat{V}$. Neutral and charge-separated states couple through the electron transfer integral t_{CT} (Figure 8), which describes the transfer of an electron between overlapping donor and acceptor moieties on neighboring molecules. We furthermore neglect electron transfer between nonoverlapping donor and acceptor moieties as the integral is expected to tend toward zero due to minimal spatial overlap. Finally, the equilibrium nuclear geometries of the ionic states are defined by an ionic Huang−Rhys parameter, λ_{CT}^2 which we set equal to 0.5, in line with the expected smaller geometric rearrangement of the ionic species compared to the zwitterion. The Hamiltonian for the system described is written as

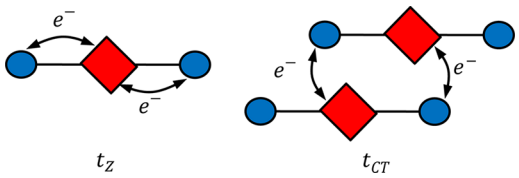

Figure 8. Illustration of the intramolecular (left) and intermolecular (right) electron transfer reactions considered in our model for squaraine. Red squares represent the central four-membered ring of the molecule while blue circles represent the nitrogen atoms on each arm.

$$\hat{H} = \sum_n \hat{H}_n^{\text{mon}} + \hat{H}^{\text{CS}} + \hat{H}^{\text{inter}} + \hat{V} \tag{5}$$

where $\hat{H}^{\text{CS}}$ defines the electronic and vibrational Hamiltonian of charge-separated states and $\hat{H}^{\text{inter}}$ defines the intermolecular electron transfer which couples neutral and charge-separated states. We note that $\hat{V}$ now also includes the Coulomb attraction between ionic species in addition to the interaction between neutral species. Again, we defer the explicit form of the Hamiltonian to the SI.

The effects of intermolecular charge transfer on the absorption spectrum are demonstrated by the red curve in Figure 7. The simulation uses the same parameters as the blue curve (Coulombically coupled aggregate) but allows for intermolecular charge transfer, setting $\eta_{CT} = 2\eta_Z$ and $t_{CT} = 0.4$ eV. It is immediately noticed that this spectrum contains a substantial low-energy component filled out with vibronic structure, reminiscent of the experimental squaraine thin film and mixed-solvent spectra in Figures 2−4. It is also significant that the high-energy peak is further blue-shifted when compared to the spectrum representing the dimer aggregate

DOI: 10.1021/acs.jpcc.5b05095
J. Phys. Chem. C 2015, 119, 18964−18974

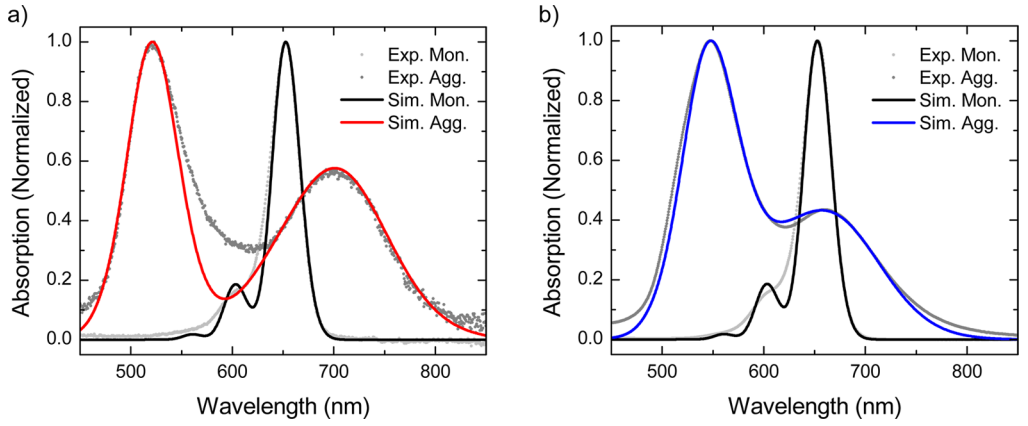

Figure 9. Simulated spectra of $DPrSQ(OH)_2$ (left) and $DBSQ(OH)_2$ (right) aggregates in 50:50 DMSO/H_2O solvent mixtures using the essential states dimer model including ICT.

without intermolecular charge transfer. These features are similar to the measured squaraine spectra in section II, which exhibit both a broad, low-energy peak and a narrower, high-energy peak. As we show next, this model is capable of faithfully reproducing the experimentally observed aggregate spectra.

Our simulated mixed-solvent spectra of both squaraine species using eq 5 are shown in Figure 9. For the simulated spectra, the dimer geometry was set according to the crystal structure while only the intermolecular charge transfer integral, t_{CT}, and ion pair energy, η_{CT}, were taken as adjustable parameters. These were set to the values that best reproduce the experiment. Furthermore, we have aligned the spectra to the most-intense peak (requiring spectral shifts of <0.1 eV) and have taken the standard deviation of the Gaussian line shape to be 0.15 eV. We point out that a consistent line width was taken for the entire spectrum and that the broadening of the low-energy peak is a result of the vibronic structure. A full list of parameters for these simulations can be found in Table 2.

Table 2. Parameters for Modeling Squaraine Mixed-Solvent Spectra

parameter	$DPrSQ(OH)_2$	$DBSQ(OH)_2$
η_Z	0.69 eV	0.69 eV
t_Z	1.05 eV	1.05 eV
λ^2	1	1
$\hbar\omega_{vib}$	0.16 eV	0.16 eV
η_{CT}	1.42 eV	1.37 eV
t_{CT}	0.55 eV	0.28 eV
λ_{CT}^2	0.5	0.5
line width	0.15 eV	0.15 eV
spectral shift	−0.087 eV	0.006 eV

The intermolecular charge transfer integral for $DPrSQ(OH)_2$ is significantly larger than that of $DBSQ(OH)_2$, a fact consistent with the roughly 0.2 Å shorter nearest-neighbor donor−acceptor distance. (See the SI for geometric parameters for the two species.) While we expect the relative magnitudes of these integrals to be consistent with the true values, we remind the reader that since we are modeling the aggregate system as a dimer, these are effective parameters representing an upper bound of the actual values. In larger stacks, most molecules have two nearest neighbors with which to couple, rather than just one as in the case of the dimer, reducing the need for such large intermolecular charge transfer integrals to reproduce the experimental spectrum. Indeed, simulations of larger rigid aggregates (no vibronic coupling) show that the t_{CT} giving the best-fit spectrum decreases continually with an increasing number of chromophores. Simulations of a six-molecule rigid aggregate, the largest our current resources allow, show that the value of t_{CT} giving the best fit is only 68% of the dimer value, approaching the 50% limit expected in an infinite aggregate where every molecule has two nearest neighbors. The magnitude of this reduced value (0.1−0.25 eV) resembles that of charge transfer integrals found in other π-stacked organic semiconducting materials and should be closer to the actual value for squaraine.

IV.4. Analysis of the Spectral Line Shape. We find that the magnitude of t_{CT} is largely responsible for the peak spacing in Figure 9 while η_{CT} is responsible for the relative peak heights. Hence, according to the experimental spectra, $DPrSQ(OH)_2$ appears to couple more strongly to the ICT state than does $DBSQ(OH)_2$. The spectral line shapes can be qualitatively understood within a rigid dimer model where vibronic coupling is neglected. We consider the eigenstates, symmetrized with respect to inversion, of the corresponding Hamiltonian for noninteracting (ni) molecules (no Coulomb or ICT interactions), which is given by

$$\hat{H}_{el}^{ni} = \sum_n \hat{H}_{el,n}^{mon} + \hat{H}_{el}^{CS} \tag{6}$$

where the index n runs over both molecules in the dimer. Details of the transformation from the diabatic basis to the basis that diagonalizes eq 6 are given in the SI. Within this basis, the spectra can be approximately described using an effective two-level system of excited states as illustrated in Figure 10. The first state of interest is the optically allowed excited state of the noninteracting dimer. This state is written as $|ge_1\rangle_{AS} = (|ge_1\rangle - |e_1g\rangle)/2^{1/2}$, where $|e_1g\rangle$ represents the state of the dimer in which molecule one is in the first excited state while molecule two is in the ground state. Note that the state is antisymmetric with respect to inversion, as are all optically allowed states. The second state of interest is an antisymmetric charge-separated state $|ac_1\rangle_{AS} = (|ac_1\rangle - |c_1a\rangle)/2^{1/2}$ where c_1 represents a linear combination of $|C_1\rangle$, $|C_2\rangle$, and $|Z_3\rangle$ states (further details in the SI) and a represents the $|A\rangle$ state. Due to the Coulomb stabilization felt by ions in the charge-separated state, $|ac_1\rangle_{AS}$ is lowered into resonance with $|ge_1\rangle_{AS}$ and the two couple via the matrix element $-2t_{CT}t_Z/(\eta_Z^2 + 8t_Z^2)^{1/2}$ due to $\hat{H}^{inter}$. Other states coupling with these two are energetically well separated

DOI: 10.1021/acs.jpcc.5b05095
J. Phys. Chem. C 2015, 119, 18964−18974

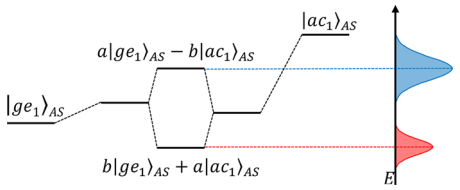

Figure 10. Illustration of the initial and mixed states in the two-level analysis. The energy-level diagram (left) shows the effect each part of the Hamiltonian has on the states of interest. The outermost levels represent the energies of the states given by eq 6 for which the states are diagonal. When the Coulomb term is added to the Hamiltonian, the energy of $|ge_1\rangle_{AS}$ increases due to the side-by-side packing of the squaraine molecules while $|ac_1\rangle_{AS}$ is stabilized due to the attraction felt by oppositely charged ions. Hence, the two states are brought into resonance by $\hat{V}$. Finally, the central levels show that the two states are mixed by $\hat{H}^{inter}$. These states are responsible for the observed absorption spectrum. The absorption intensity to each mixed state (right) depends on the coefficient weighting the $|ge_1\rangle_{AS}$ component of the state. In this illustration, $|ac_1\rangle_{AS}$ has a lower energy than $|ge_1\rangle_{AS}$ so that the low-energy peak has more $|ac_1\rangle_{AS}$ character and is less intense than the higher-energy peak.

and are neglected here, though they are expected to have minor effects.

In the symmeterized basis, $|ge_1\rangle_{AS}$ possesses all of the oscillator strength given that $|gg\rangle_S$ defines the ground state; i.e., the ground state is given by the direct product of ground states arising from the solution of eq 1. When $|ge_1\rangle_{AS}$ and $|ac_1\rangle_{AS}$ mix to form the excited states of the system, the resulting states each acquire some oscillator strength due to their $|ge_1\rangle_{AS}$ component, resulting in a double-hump feature in the absorption spectrum. Hence, the excited states of squaraine aggregates can be characterized by analyzing their absorption spectra. The relative intensity of each peak gives information about the makeup of the optically active excited states. The peak with the largest oscillator strength has more neutral $|ge_1\rangle_{AS}$ character, while the peak with the smaller oscillator strength has more ionic $|ac_1\rangle_{AS}$ character. At the same time, the peak spacing gives information about the intermolecular charge transfer integral, t_{CT}, and hence the ability of the system to form a charge-separated state. This may have implications for organic photovoltaic devices which require efficient charge separation and could offer a quick screening method to identify viable candidates though an analysis of the absorption spectrum. Systems that exhibit a two-peak absorption spectrum with a large peak-to-peak spacing and similar peak intensities should readily form intermolecular charge-separated states.

While our simulations faithfully reproduce the main spectral features of the experiment, there remains room for improvement. In the $DPrSQ(OH)_2$ spectra, for instance, the simulations are missing intensity in the gap between the two peaks. Preliminary calculations of larger aggregates composed of rigid squaraine molecules suggest that this intensity gap is a result of the finite size of the dimer as this region begins to fill in with increasing aggregate size. Nevertheless, we have found it necessary to utilize (homogeneous) Gaussian line shapes for aggregate transitions roughly twice as broad as those used to reproduce the monomer spectrum. Moreover, we observe more optically allowed states in our simulations as the size of the aggregate grows. If a consideration of substantially larger aggregate sizes were within our computational reach, then the large line width would likely resolve to a more reasonable value. The investigation of these interesting size effects is ongoing and will be presented in a future publication.

V. CONCLUSIONS

In this work we have shown that the broad, double-peaked nature of the absorption spectra of aggregates and thin films of the squaraine dyes, $DPrSQ(OH)_2$ and $DBSQ(OH)_2$, is due to intermolecular charge transfer. The spectra cannot be explained by conventional exciton theory in terms of H- and J-aggregation as originally proposed by Kasha.[25] Our model is consistent with the crystal structure of both dyes which places a nitrogen atom of one molecule in close proximity to the squarylium moiety of a neighboring molecule within the tightly packed π-stack. Charge transfer between the nitrogen and the four-membered ring is consistent with the findings of Tristani-Kendra and Eckhardt,[17] who analyzed polarized absorption in thin films of a related squaraine, DESQ(OH), the triclinic form of which packs in a similar fashion to $DPrSQ(OH)_2$ and $DBSQ(OH)_2$.

To fully account for the absorption spectral line shapes of $DPrSQ(OH)_2$ and $DBSQ(OH)_2$ in solution and in the solid phase, we employed the essential state model pioneered by Painelli and co-workers[16] to model a monomeric squaraine and subsequently added ICT and Coulomb coupling in order to model aggregates. We found that through-space Coulombic interactions alone, as exist in conventional Frenkel exciton theory, cannot satisfactorily reproduce the aggregate spectra. We subsequently confirmed that ICT plays a major role in determining the distinct absorption spectral signatures of $DPrSQ(OH)_2$ and $DBSQ(OH)_2$ aggregates. We point out that not all squaraines exhibit evidence of ICT; in particular, the monoclinic phase of DESQ(OH), which, unlike the triclinic phase hosts two molecules per unit cell, shows clear evidence of Davydov splitting but no ICT. Not only do we remedy any confusion regarding the origin of the panchromatic solid-state features in certain squaraines, which is critical for a substantial overlap of the solar spectrum, but with a full understanding of the excited-state assignment, we also provide a foundation for understanding the impact of aggregation on OPV device efficiency.

■ ASSOCIATED CONTENT

Supporting Information

The Supporting Information is available free of charge on the ACS Publications website at DOI: 10.1021/acs.jpcc.5b05095.

Additional absorption and fluorescence spectra, a description of the Hamiltonian, the dipole moments and the modeled absorption spectra, and a larger analysis of the origin of the double peaked spectra are provided in Supporting Information. (PDF)
ritjc02. (CIF)
ritjc01. (CIF)

■ AUTHOR INFORMATION

Corresponding Author

*E-mail: cjcscha@rit.edu.

Author Contributions

The manuscript was written through the contributions of all authors. All authors have given approval to the final version of the manuscript.

Notes

The authors declare no competing financial interest.

DOI: 10.1021/acs.jpcc.5b05095
J. Phys. Chem. C 2015, 119, 18964−18974

■ ACKNOWLEDGMENTS

We acknowledge Patrick Cost, Patrick Heaphy, and Kyle Oliver for help in synthesizing the squaraine compounds. We also acknowledge Susan Spencer for her broad expertise in squaraines, many fruitful discussions, and much preliminary device data that generated so much interest in these materials. We gratefully acknowledge William W. Brennessel and the X-ray Crystallographic Facility of the Department of Chemistry at the University of Rochester for XRD data. The initial instrument purchase was through NSF grant CHE-9422567, and the upgrade was through NSF grant CHE-0342508. We acknowledge funding from the Department of Energy (DOE DE-FG36-08GO88110) and the National Science Foundation (CBET-1236372 and IIP-1237761).

■ REFERENCES

(1) Makowski, B. T.; Valle, B.; Singer, K. D.; Weder, C. A Melt-Processable Squaraine-Based Organic Glass for Nonlinear Optics. *J. Mater. Chem.* **2012**, *22*, 2848−2850.
(2) Prabhakar, C.; Bhanuprakash, K.; Rao, V. J.; Balamuralikrishna, M.; Rao, D. N. Third Order Nonlinear Optical Properties of Squaraine Dyes Having Absorption below 500 Nm: A Combined Experimental and Theoretical Investigation of Closed Shell Oxyallyl Derivatives. *J. Phys. Chem. C* **2010**, *114*, 6077−6089.
(3) Umezawa, K.; Citterio, D.; Suzuki, K. Water-Soluble NIR Fluorescent Probes Based on Squaraine and Their Application for Protein Labeling. *Anal. Sci.* **2008**, *24*, 213−217.
(4) Escobedo, J. O.; Rusin, O.; Lim, S.; Strongin, R. M. NIR Dyes for Bioimaging Applications. *Curr. Opin. Chem. Biol.* **2010**, *14*, 64.
(5) Avirah, R. R.; Jayaram, D. T.; Adarsh, N.; Ramaiah, D. Squaraine Dyes in PDT: From Basic Design to in Vivo Demonstration. *Org. Biomol. Chem.* **2012**, *10*, 911−920.
(6) Luo, C.; Zhou, Q.; Jiang, G.; He, L.; Zhang, B.; Wang, X. The Synthesis and 1O2 Photosensitization of Halogenated Asymmetric Aniline-Based Squaraines. *New J. Chem.* **2011**, *35*, 1128−1132.
(7) Beverina, L.; Salice, P. Squaraine Compounds: Tailored Design and Synthesis towards a Variety of Material Science Applications. *Eur. J. Org. Chem.* **2010**, *2010*, 1207−1225.
(8) Ajayaghosh, A. Chemistry of Squaraine-Derived Materials: Near-IR Dyes, Low Band Gap Systems, and Cation Sensors. *Acc. Chem. Res.* **2005**, *38*, 449−459.
(9) Spencer, S.; Cody, J.; Misture, S.; Cona, B.; Heaphy, P.; Rumbles, G.; Andersen, J.; Collison, C. Critical Electron Transfer Rates for Exciton Dissociation Governed by Extent of Crystallinity in Small Molecule Organic Photovoltaics. *J. Phys. Chem. C* **2014**, *118*, 14840−14847.
(10) Spencer, S.; Hu, H.; Li, Q.; Ahn, H.-Y.; Qaddoura, M.; Yao, S.; Ioannidis, A.; Belfield, K.; Collison, C. J. Controlling J-Aggregate Formation for Increased Short-Circuit Current and Power Conversion Efficiency with a Squaraine Donor. *Prog. Photovoltaics* **2014**, *22*, 488−493.
(11) Spencer, S. D.; Bougher, C.; Heaphy, P. J.; Murcia, V. M.; Gallivan, C. P.; Monfette, A.; Andersen, J. D.; Cody, J. A.; Conrad, B. R.; Collison, C. J. The Effect of Controllable Thin Film Crystal Growth on the Aggregation of a Novel High Panchromaticity Squaraine Viable for Organic Solar Cells. *Sol. Energy Mater. Sol. Cells* **2013**, *112*, 202−208.
(12) Chen, G.; Sasabe, H.; Sasaki, Y.; Katagiri, H.; Wang, X.-F.; Sano, T.; Hong, Z.; Yang, Y.; Kido, J. A Series of Squaraine Dyes: Effects of Side Chain and the Number of Hydroxyl Groups on Material Properties and Photovoltaic Performance. *Chem. Mater.* **2014**, *26*, 1356.
(13) Schwenn, P. E.; Gui, K.; Zhang, Y.; Burn, P. L.; Meredith, P.; Powell, B. J. Kinetics of Charge Transfer Processes in Organic Solar Cells: Implications for the Design of Acceptor Molecules. *Org. Electron.* **2012**, *13*, 2538−2545.
(14) Coffey, D. C.; Larson, B. W.; Hains, A. W.; Whitaker, J. B.; Kopidakis, N.; Boltalina, O. V.; Strauss, S. H.; Rumbles, G. An Optimal Driving Force for Converting Excitons into Free Carriers in Excitonic Solar Cells. *J. Phys. Chem. C* **2012**, *116*, 8916−8923.
(15) Bigelow, R. W.; An, H.-J. F. MNDO and CNDO/S(S DES CI) Study on the Structural and Electronic Properties of a Model Squaraine Dye and Related Cyanine. *Chem. Phys.* **1986**, *107*, 159−174.
(16) Terenziani, F.; Painelli, A.; Katan, C.; Charlot, M.; Blanchard-Desce, M. Charge Instability in Quadrupolar Chromophores: Symmetry Breaking and Solvatochromism. *J. Am. Chem. Soc.* **2006**, *128*, 15742−15755.
(17) Tristani-Kendra, M.; Eckhardt, C. J. Influence of Crystal Fields on the Quasimetallic Reflection Spectra of Crystals: Optical Spectra of Polymorphs of a Squarylium Dye. *J. Chem. Phys.* **1984**, *81*, 1160−1173.
(18) Tanaka, J.; Tanaka, M.; Hayakawa, M. Electronic Spectra of Single Crystals of 1,1'-Diethyl-2,2'-Cyanine Iodide, Bromide, and Chloride. *Bull. Chem. Soc. Jpn.* **1980**, *53*, 3109−3119.
(19) Zhang, Y.; Kim, B.; Yao, S.; Bondar, M. V.; Belfield, K. D. Controlled Aggregation and Enhanced Two-Photon Absorption of a Water-Soluble Squaraine Dye with a Poly(acrylic Acid) Template. *Langmuir* **2013**, *29*, 11005−11012.
(20) Gräf, K.; Rahim, M. A.; Das, S.; Thelakkat, M. Complementary Co-Sensitization of an Aggregating Squaraine Dye in Solid-State Dye-Sensitized Solar Cells. *Dyes Pigm.* **2013**, *99*, 1101−1106.
(21) Pisoni, D. d. S.; de Abreu, M. P.; Petzhold, C. L.; Rodembusch, F. S.; Campo, L. F. Synthesis, Photophysical Study and BSA Association of Water-Insoluble Squaraine Dyes. *J. Photochem. Photobiol., A* **2013**, *252*, 77−83.
(22) Deing, K. C.; Mayerhöffer, U.; Würthner, F.; Meerholz, K. Aggregation-Dependent Photovoltaic Properties of squaraine/PC61BM Bulk Heterojunctions. *Phys. Chem. Chem. Phys.* **2012**, *14*, 8328.
(23) Spano, F. C. The Spectral Signatures of Frenkel Polarons in H- and J-Aggregates. *Acc. Chem. Res.* **2010**, *43*, 429−439.
(24) Spano, F. C. Analysis of the UV/Vis and CD Spectral Line Shapes of Carotenoid Assemblies: Spectral Signatures of Chiral H-Aggregates. *J. Am. Chem. Soc.* **2009**, *131*, 4267−4278.
(25) Kasha, M.; Rawls, H. R.; Ashraf El-Bayoumi, M. The Exciton Model in Molecular Spectroscopy. *Pure Appl. Chem.* **1965**, *11*, 371−392.
(26) Spano, F. C.; Clark, J.; Silva, C.; Friend, R. H. Determining Exciton Coherence from the Photoluminescence Spectral Line Shape in poly(3-Hexylthiophene) Thin Films. *J. Chem. Phys.* **2009**, *130*, 074904.
(27) Shafeekh, K. M.; Das, S.; Sissa, C.; Painelli, A. Asymmetric Squaraine Dyes: Spectroscopic and Theoretical Investigation. *J. Phys. Chem. B* **2013**, *117*, 8536−8546.
(28) D'Avino, G.; Terenziani, F.; Painelli, A. Aggregates of Quadrupolar Dyes: Giant Two-Photon Absorption from Biexciton States. *J. Phys. Chem. B* **2006**, *110*, 25590−25592.
(29) Sissa, C.; Terenziani, F.; Painelli, A.; Abbotto, A.; Bellotto, L.; Marinzi, C.; Garbin, E.; Ferrante, C.; Bozio, R. Dimers of Quadrupolar Chromophores in Solution: Electrostatic Interactions and Optical Spectra. *J. Phys. Chem. B* **2010**, *114*, 882−893.
(30) Terenziani, F.; D'Avino, G.; Painelli, A. Multichromophores for Nonlinear Optics: Designing the Material Properties by Electrostatic Interactions. *ChemPhysChem* **2007**, *8*, 2433−2444.
(31) Terenziani, F.; Painelli, A. Supramolecular Interactions in Clusters of Polar and Polarizable Molecules. *Phys. Rev. B: Condens. Matter Mater. Phys.* **2003**, *68*, 165405.
(32) Terenziani, F.; Painelli, A. Collective and Cooperative Phenomena in Molecular Materials: Dimers of Polar Chromophores. *J. Lumin.* **2005**, *112*, 474−478.
(33) Bakalis, L. D.; Knoester, J. Optical Properties of One-Dimensional Exciton Systems: Beyond the Heitler-London Approximation. *J. Chem. Phys.* **1997**, *106*, 6964−6976.
(34) Zheng, C.; Penmetcha, A. R.; Cona, B.; Spencer, S. D.; Zhu, B.; Heaphy, P. J.; Cody, J. A.; Collison, C. The Contribution of Aggregate

DOI: 10.1021/acs.jpcc.5b05095
J. Phys. Chem. C 2015, 119, 18964−18974

States and Energetic Disorder to a Squaraine System Targeted for Organic Photovoltaic Devices. *Langmuir* **2015**, *31*, 7717.
(35) Dirk, C. W.; Herndon, W. C.; Cervantes-Lee, F.; Selnau, H.; Martinez, S.; Kalamegham, P.; Tan, A.; Campos, G.; Velez, M. Squarylium Dyes: Structural Factors Pertaining to the Negative Third-Order Nonlinear Optical Response. *J. Am. Chem. Soc.* **1995**, *117*, 2214−2225.
(36) Tian, M.; Furuki, M.; Iwasa, I.; Sato, Y.; Pu, L. S.; Tatsuura, S. Search for Squaraine Derivatives That Can Be Sublimed without Thermal Decomposition. *J. Phys. Chem. B* **2002**, *106*, 4370−4376.
(37) Brück, S.; Krause, C.; Turrisi, R.; Beverina, L.; Wilken, S.; Saak, W.; Lützen, A.; Borchert, H.; Schiek, M.; Parisi, J. Structure−property Relationship of Anilino-Squaraines in Organic Solar Cells. *Phys. Chem. Chem. Phys.* **2014**, *16*, 1067−1077.
(38) Liang, K.; Law, K.-Y.; Whitten, D. G. Multiple Aggregation of Surfactant Squaraines in Langmuir-Blodgett Films and in DMSO-Water Mixtures. *J. Phys. Chem.* **1994**, *98*, 13379−13384.
(39) Kim, S.; Furuki, M.; Pu, L. S.; Nakahara, H.; Fukuda, K. Unique Monolayer Assembly of Squarylium Dye with Short Alkyl Chains. *J. Chem. Soc., Chem. Commun.* **1987**, 1201−1203.
(40) Tanaka, M.; Sekiguchi, T.; Matsumoto, M.; Nakamura, T.; Manda, E.; Kawabata, Y. The Spontaneous Formation of a J-like Aggregate in Langmuir-Blodgett Films of a Squarylium Dye. *Thin Solid Films* **1988**, *160*, 299−302.
(41) Iwamoto, M.; Majima, Y.; Hirayama, F.; Furuki, M.; Pu, L. S. Generation of the Displacement Current by the Transformation of J-Aggregates in Spreading Monolayers of Squarylium Dye. *Chem. Phys. Lett.* **1992**, *195*, 45−49.
(42) McKerrow, A. J.; Buncel, E.; Kazmaier, P. M. Aggregation of Squaraine Dyes: Structure−property Relationships and Solvent Effects. *Can. J. Chem.* **1995**, *73*, 1605−1615.
(43) Collison, C. J.; Rothberg, L. J.; Treemaneekarn, V.; Li, Y. Conformational Effects on the Photophysics of Conjugated Polymers: A Two Species Model for MEH−PPV Spectroscopy and Dynamics. *Macromolecules* **2001**, *34*, 2346−2352.
(44) Yamagata, H.; Pochas, C. M.; Spano, F. C. Designing J- and H-Aggregates through Wave Function Overlap Engineering: Applications to poly(3-Hexylthiophene). *J. Phys. Chem. B* **2012**, *116*, 14494−14503.
(45) Kuwata-Gonokami, M.; Peyghambarian, N.; Meissner, K.; Fluegel, B.; Sato, Y.; Ema, K.; Shimano, R.; Mazumdar, S.; Guo, F.; Tokihiro, T.; et al. Exciton Strings in an Organic charge transfer Crystal. *Nature* **1994**, *367*, 47−48.
(46) Law, K. Y. Organic Photoconductive Materials: Recent Trends and Developments. *Chem. Rev.* **1993**, *93*, 449−486.
(47) Guasch, J.; Grisanti, L.; Souto, M.; Lloveras, V.; Vidal-Gancedo, J.; Ratera, I.; Painelli, A.; Rovira, C.; Veciana, J. Intra- and Intermolecular Charge Transfer in Aggregates of Tetrathiafulvalene-Triphenylmethyl Radical Derivatives in Solution. *J. Am. Chem. Soc.* **2013**, *135*, 6958−6967.

DOI: 10.1021/acs.jpcc.5b05095
J. Phys. Chem. C 2015, 119, 18964−18974